

Obesity fosters severe disease outcomes in a mouse model of coronavirus infection associated with transcriptomic abnormalities

Pallavi Rai¹, Jeffrey M. Marano², Lin Kang¹, Sheryl Coutermarsh-Ott¹, Andrea Daamen³, Peter Lipsky E³, and James Weger-Lucarelli¹

¹Virginia-Maryland College of Veterinary Medicine Department of Biomedical Sciences and Pathobiology

²Center for Emerging Zoonotic and Arthropod-borne Pathogens Virginia Tech

³AMPEL BioSolutions LLC

March 13, 2024

Abstract

Obesity has been identified as an independent risk factor for severe outcomes in humans with coronavirus disease 2019 (COVID-19) and other infectious diseases. Here, we established a mouse model of COVID-19 using the murine betacoronavirus, mouse hepatitis virus 1 (MHV-1). C57BL/6 and C3H/HeJ mice exposed to MHV-1 developed mild and severe disease, respectively. Obese C57BL/6 mice developed clinical manifestations similar to those of lean controls. In contrast, all obese C3H/HeJ mice succumbed by 8 days post-infection, compared to a 50% mortality rate in lean controls. Notably, both lean and obese C3H/HeJ mice exposed to MHV-1 developed lung lesions consistent with severe human COVID-19, with marked evidence of diffuse alveolar damage (DAD). To identify early predictive biomarkers of worsened disease outcomes in obese C3H/HeJ mice, we sequenced RNA from whole blood 2 days post-infection and assessed changes in gene and pathway expression. Many pathways uniquely altered in obese C3H/HeJ mice post-infection aligned with those found in humans with severe COVID-19. Furthermore, we observed altered gene expression related to the unfolded protein response and lipid metabolism in infected obese mice compared to their lean counterparts, suggesting a role in the severity of disease outcomes. This study presents a novel model for studying COVID-19 and elucidating the mechanisms underlying severe disease outcomes in obese and other hosts.



Introduction

Severe acute respiratory syndrome coronavirus 2 (SARS-CoV-2), the virus responsible for COVID-19, remains a global epidemiological concern as it continues to give rise to new variants exhibiting increased transmissibility and disease-causing potential^{1,2}. As of 14th January, 2024, SARS-CoV-2 was responsible for ~774 million confirmed cases and ~7 million deaths globally and ~103 million confirmed cases and 1.2 million deaths in the U.S. alone³. The clinical manifestations range from mild respiratory symptoms to pneumonia, and in most severe instances, multi-organ failure and death⁴. Several epidemiological studies have shown strong associations between disease severity and co-morbidities, such as hypertension, diabetes, old age, cardiovascular diseases, and obesity⁵⁻¹¹. More severe cases and deaths related to COVID-19 have been associated with macrophage activation¹², caused by a dysregulated host immune response¹³.

Obesity has been identified as an independent risk factor for severe COVID-19¹⁴⁻¹⁸ and has been associated with chronic systemic inflammation^{19,20}. However, most of these inferences are correlative and are based either on data from epidemiological studies^{7,8,11,15,17} or from studies performed in non-natural hosts of SARS-CoV-2^{21,22}. Therefore, a relevant model of coronavirus infection, which mimics SARS-CoV-2 infection in humans, is needed to study the impact of obesity on coronavirus disease outcome. We hypothesized that this model would be useful for identifying biomarkers associated with disease severity in COVID-19 patients, which could have prognostic value for risk stratification of patients with COVID-19.

To this end, we used C57BL/6N and C3H/HeJ mouse models of diet-induced obesity and inoculated them with mouse hepatitis virus 1 (MHV-1), a pneumotropic betacoronavirus which has been previously used to study SARS-CoV-1 infection²³⁻²⁵. We observed more severe disease in obese C3H/HeJ mice exposed to MHV-1 including increased weight loss, mortality, and tissue pathology. Moreover, RNA sequencing

(RNAseq) analysis of whole blood RNA showed commonly altered genes and pathways between MHV-1 infected obese C3H/HeJ mice and humans with severe COVID-19 suggesting the relevance of our mouse model in identifying biomarkers of severe COVID-19 disease outcomes.

Materials and Methods

Mice and diets

Male and female C57BL/6N mice from Charles River Laboratories (Boston, MA, USA) and C3H/HeJ mice from The Jackson Laboratory (Bar Harbor, ME, USA) were obtained at three to four weeks of age and allowed to acclimatize for a week before initiating diets. Mice were housed in groups of five per cage and maintained at ambient temperature with *ad libitum* supply of food and water. All animal handling protocols were approved by the Institutional Animal Care and Use Committee (Protocol #20-060) at Virginia Tech.

All diets used for the study were obtained from Research Diets (New Brunswick, NJ, USA). Males and females of both strains were randomly divided and half of them were given a low-fat diet with 10% kcal fat (LFD; D12450K), while the other half were given a high-fat diet with 60% kcal fat (HFD; D12492). Throughout the manuscript, we will refer to the groups as follows: lean (low fat diet) or obese (high fat diet). The mice were kept on these diets for 17-18 weeks before infections, and the same diets were continued until the end of the experiment.

Glucose levels

Two weeks prior to MHV-1 inoculations (16 weeks after diet initiation), mice bled via submandibular bleeds and non-fasting glucose levels were measured at 9-10 am using the Abox glucose monitoring kit.

Mouse infections and health monitoring

Mice were transferred to disposable cages from Innovive (San Diego, CA, USA) and moved to a separate room, 3-4 days before MHV-1 infection. MHV-1 was a kind gift from Dr. Susan Compton and was propagated in 17C11 cells; infectious titers were determined by plaque assays on L2 Percy cells. Mice were anesthetized with ketamine and xylazine (90 mg/kg and 5 mg/kg respectively) intraperitoneally and then inoculated intranasally with 3×10^4 plaque-forming units (PFUs) of the virus in 50 μ L of Roswell Park Memorial Institute (RPMI)-1640 media with no additives or only 50 μ L of RPMI-1640 (mock-infection). Mice were monitored for visual symptoms of disease like inactivity, weight loss and mortality. They were euthanized at 8 dpi or when they crossed the threshold of weight loss (20% of weights at 0 dpi), by injecting ketamine and xylazine (90 mg/kg and 10 mg/kg respectively) intraperitoneally followed by cervical dislocation. For histopathology, the left lung lobe was perfused with and stored in 4% formaldehyde for at least a week. We also collected sections of the liver, spleen, and small intestine for histopathological analyses. The Virginia Tech Animal Laboratory Services (ViTALS) performed paraffin embedding, sectioning and hematoxylin-eosin staining, and a board-certified pathologist scored the slides in a blinded manner.

RNA extraction from whole blood

Mice were anesthetized with ketamine and xylazine (90 mg/kg and 5 mg/kg respectively) intraperitoneally and 100 μ L of whole blood was collected via submandibular cheek bleeds, in EDTA coated tubes. We added 300 μ L of TRIzol LS reagent (ThermoFisher) to each tube and total RNA was extracted using the manufacturer's protocol and stored at -80°C until use.

RNA sequencing and pathway enrichment data analysis

RNA from the whole blood of 16 MHV-1- and 16 mock-infected C3H/HeJ mice were submitted to BGI (Cambridge, MA, USA) to perform library prep and sequencing using their DNBseq platform. RNA quality was assessed using Nanodrop 260/280 and 260/230 ratios and raw reads were generated as Fastq files. We performed quality control on the raw reads using FastQC²⁶ and trimmed them using BBDuk²⁷. The mouse reference genome (GRCm39) and corresponding annotations were downloaded from National Center for Biotechnology Information (NCBI, Bethesda, MD, USA). The clean reads were mapped to the reference

genome using the Spliced Transcripts Alignment to a Reference (STAR) with default parameters²⁸. HT-Seq (htseq-count) within the STAR package was used to estimate gene counts²⁹. Differential gene expression analysis was conducted using DESeq2³⁰, and Gene Set Enrichment Analysis (GSEA) was performed using the Kyoto Encyclopedia of Genes and Genomes (KEGG) database. We employed the integrated differential expression and pathway analysis tool (iDEP 0.96, South Dakota University, SD, USA)³¹ for these analyses, setting the default parameters to a p-adjusted value of <0.1 and fold change of >2 for identifying differentially expressed genes. The expression patterns of identified biomarker genes were plotted with gene plot feature in iDEP 2.0 using raw counts and standard deviation.

Gene set variation analysis (GSVA)

The R/Bioconductor software package GSVA³² was used as a non-parametric, unsupervised method to estimate enrichment of immune cell and pathway gene sets in RNAseq data as previously described^{12,33,34}. Gene sets used as input for GSVA can be found in Supplementary Table 2.

Statistical analysis

Statistical and regression analyses were done using GraphPad Prism 9 (GraphPad Software, San Diego, CA, USA). Details of the statistical technique used for the analyses are provided in the figure legends. The level of significance has been determined by the following p-values: p [?] 0.05 (ns); p = 0.05 to 0.01 (*); p = 0.01 to 0.001 (**); p = 0.001 to 0.0001 (***); p < 0.0001 (****). The error bars represent standard deviation from the mean and the dotted lines denote the limit of detection (L.O.D.). All statistical analyses were performed on data after testing them for normality using the Shapiro-Wilk test.

Results and Discussion

C3H/HeJ mice fed a high fat diet develop diet-induced obesity (DIO) similar to C57BL/6N mice. Based on previous literature and preliminary studies, we identified C57BL/6N and C3H/HeJ mice as resistant and susceptible models, respectively, to mouse hepatitis virus 1 (MHV-1)^{35,36}. C57BL/6N mice are an established model of diet-induced obesity (DIO)³⁷ and experience mild disease following MHV-1 infection³⁸. Numerous studies have demonstrated that C3H/HeJ mice—which experience severe disease following MHV-1 exposure—exhibit resistance to DIO³⁹⁻⁴¹. Conversely, other research has indicated that they exhibit dietary responses similar to C57BL/6N mice⁴². Therefore, to establish a model of obesity for studying its impact on MHV-1 infection, we used both mouse strains. C57BL/6N and C3H/HeJ mice fed a high-fat diet (HFD) had significantly higher weights compared to those on a low-fat diet (LFD) from 2-weeks-post-diet-initiation (Fig.1A & B, **p=0.0010 and **p=0.0030 respectively), which gradually became more significant by 18 weeks (Fig.1A & B, ****p<0.0001). Non-fasting glucose levels at 16-weeks-post-diet-initiation were significantly higher in obese mice compared to their lean counterparts in both, C57BL/6N and C3H/HeJ mice (Fig.1C & D, ***p<0.0001 and ***p=0.0005). This 18-week diet regimen produced C57BL/6N and C3H/HeJ mice that mirrored obesity and hyperglycemia in humans and, therefore, were appropriate to study the effect of obesity on coronavirus infection.

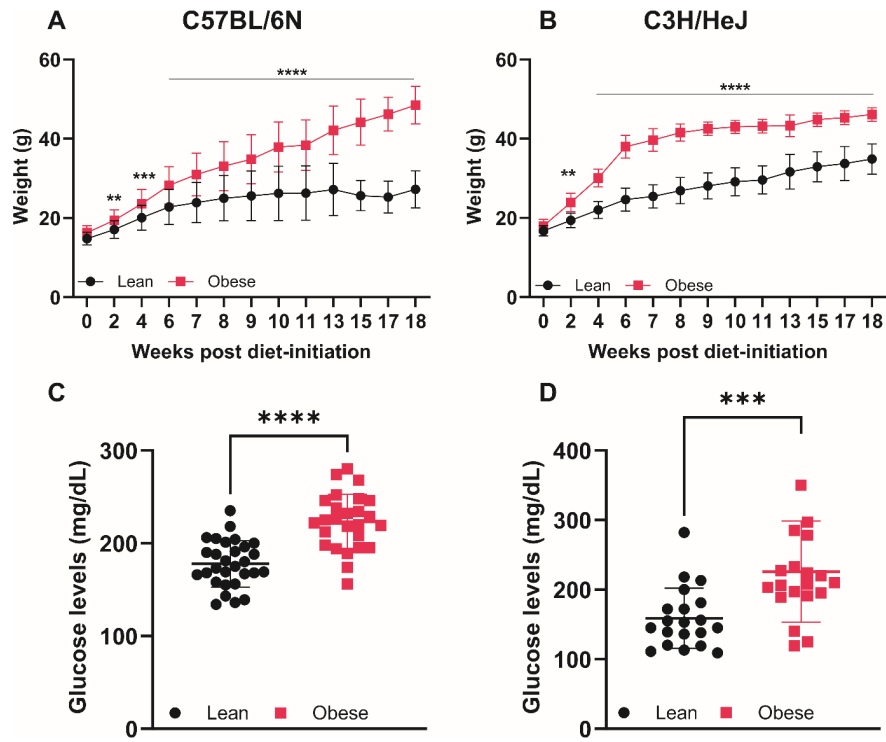


Fig.1: C57BL/6N and C3H/HeJ mice on a high fat diet develop diet-induced obesity (DIO).

Four-week-old C57BL/6N (n=22-23) and C3H/HeJ (n=14-20) were fed a HFD (60% fat) or a LFD (10% fat) for 18 weeks. **(A & B) Weight gain in lean and obese C57BL/6N and C3H/HeJ mice respectively.** Weights were measured throughout the feeding period and statistical analysis was carried out using mixed effects analysis with Sidak's multiple comparisons test. **(C & D) Glucose levels in lean and obese C57BL/6N and C3H/HeJ mice respectively.** Two weeks before infection (16-weeks-post-diet-initiation), blood was collected by submandibular cheek bleeds and non-fasting glucose levels were measured. Statistical analysis was done using an unpaired t-test. The level of significance is represented as follows: $p < 0.001$ (**); $p = 0.001$ to 0.0001 (***) ; $p < 0.0001$ (****). The error bars indicate the standard deviation (SD) of the mean.

Obese C3H/HeJ mice exposed to MHV-1 experience more severe disease outcomes compared to C57BL/6N mice. Since its outbreak in 2019, severe COVID-19 outcomes have been strongly and independently correlated with obesity⁴³, with severe obesity leading to 3.6 times more ICU admissions¹⁷. Obesity significantly increased the risk of mortality in young COVID-19 patients¹¹ and has been shown in COVID-19 patients across the world⁴⁴⁻⁴⁶. To determine the impact of obesity on disease severity and identify an appropriate mouse model for studying coronavirus pathogenesis and biomarker discovery, lean and obese C57BL/6N and C3H/HeJ mice were inoculated intranasally with 3×10^4 PFUs of MHV-1 and monitored for weight loss, mortality, and other signs of illness until 8 days-post-infection (dpi) (Fig.2A) when mice were euthanized to collect tissues for histopathology.

Obese C57BL/6N mice inoculated with MHV-1 showed significantly greater weight loss compared to their lean counterparts at 2 and 8 dpi (Fig.2B, ** $p=0.0029$; * $p=0.0483$, respectively). More strikingly, obese C3H/HeJ mice showed significantly higher weight loss at 1, 2, 6 and 7 dpi (Fig.2C, *** $p=0.0004$, ** $p=0.0018$, * $p=0.0472$ and * $p=0.0290$, respectively). There was no difference in the survival up to 8 dpi between lean and obese C57BL/6N mice (Fig.2D); in contrast, obese C3H/HeJ mice had 100% mortality by 8 dpi (Fig.2E, *** $p=0.0002$) compared to 50% mortality in lean mice. The significant weight loss and mortality rates in our obese C3H/HeJ mice inoculated with MHV-1, therefore, mirror the morbidity and mortality observed in

obese humans suffering from COVID-19, suggesting the relevance of our infection model to study COVID-19 in the context of obesity.

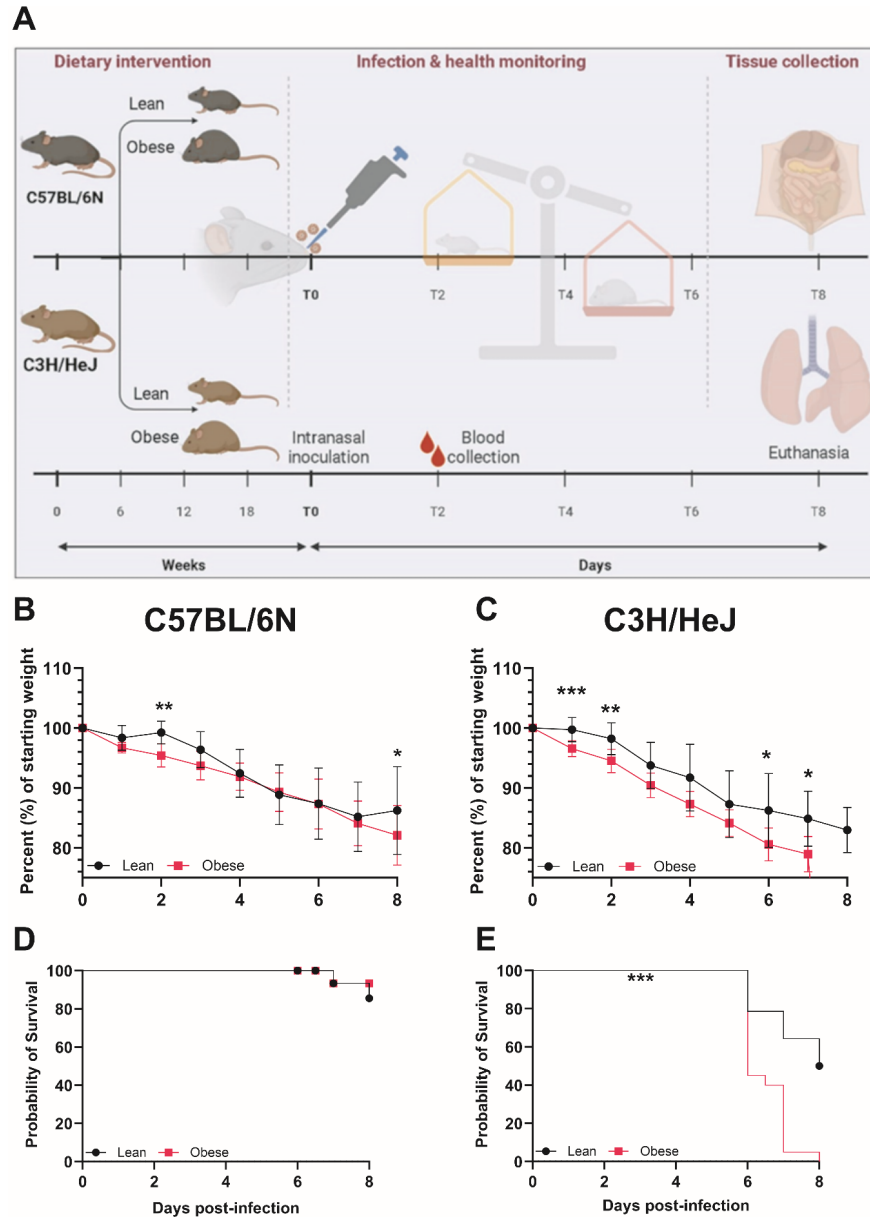
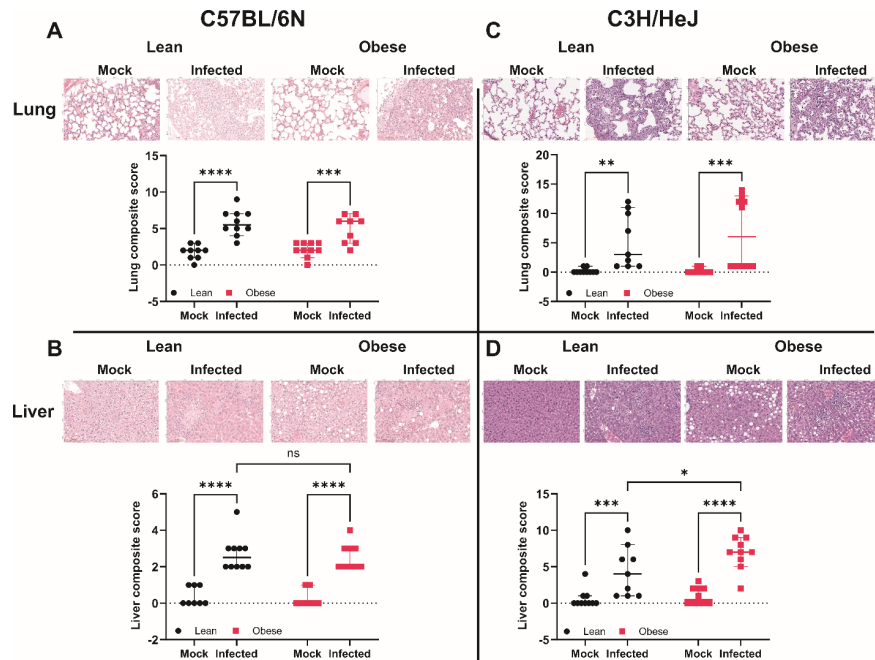


Fig.2: Obese C3H/HeJ mice exposed to MHV-1 have worse disease outcomes compared to C57BL/6N mice.

(A) Experimental design. Lean and obese C57BL/6N ($n=20-25$) and C3H/HeJ ($n=15-20$) mice were intranasally inoculated with 3×10^4 PFUs of MHV-1 at 18-weeks-post-diet-initiation (day 0). The mice were bled at 2 dpi and monitored for signs of illness, weight loss and mortality until 8 dpi. At 8 dpi, the remaining mice were euthanized, and tissues were collected for histopathology. **(B & C) Weight changes in lean and obese C57BL/6N (B) and C3H/HeJ (C) mice.** Weights were measured daily, and statistical analysis was done on baseline corrected weights using mixed effects analysis with Sidak's multiple comparisons test.

(D & E) Survival rates in lean and obese C57BL/6N (D) and C3H/HeJ (E) mice. Infected lean and obese mice were monitored until 8 dpi. Mortality was recorded if a mouse succumbed to infection or reached criteria for humane euthanasia (20% weight loss compared to weights at 0 dpi). Statistical analysis was done using Log-rank (Mantel-Cox) test. The level of significance is represented as follows: $p < 0.05$ (*); $p < 0.001$ (**); $p = 0.001$ to 0.0001 (***) ; $p < 0.0001$ (****). The error bars indicate standard deviation (SD) of the mean. The studies were carried out as two independent replicates each for C3H/HeJ and C57BL/6N mice.



We next sought to determine the impact of MHV-1 infection on tissue pathology by examining the lungs and liver of C57BL/6N and C3H/HeJ mice that had been euthanized with more than 20% weight loss or at 8 dpi when the study was terminated (Fig.2A). Lung damage was assessed by identifying and semi-quantitatively scoring inflammation involving the alveolar septa, alveolar space, and surrounding vessels as well as the presence and degree of type II pneumocyte hyperplasia. Liver damage was assessed by identifying and semi-quantitatively scoring hepatocyte vacuolation, hepatocyte necrosis, and overall liver inflammation. The individual parameters were then summed to obtain a composite histopathologic score for each organ. In C57BL/6N mice, no differences were observed between infected lean and obese mice in either tissue (Fig.3A & B). In C3H/HeJ mice, no differences were observed in the lungs of infected obese and lean mice (Fig.3C), whereas the composite liver scores were significantly higher in obese compared to lean mice (Fig.3D, * $p=0.0260$).

Fig.3: MHV-1 infection causes severe liver pathology in obese C3H/HeJ mice.

Lean and obese C57BL/6N and C3H/HeJ mice exposed to MHV-1 were euthanized at 8 dpi or when they crossed the threshold of weight loss (20% of the baseline), and tissues were collected for histopathological analysis. H&E-stained images were captured at 20X, scale bar = 100 μ m. **Lung (A) & liver (B) histopathology of C57BL/6N mice.** Lungs (top image) and livers (bottom image) from mock and MHV-1 infected lean and obese C57BL/6N mice, showed no significant difference in histopathological lesions between both the groups. **Lung (C) & liver (D) histopathology of C3H/HeJ mice.** Lungs (top image) and livers (bottom image) from mock and MHV-1 infected lean and obese C3H/HeJ mice were examined. Statistical analysis was carried out by 2way ANOVA. The level of significance is represented as follows: $p <$

0.05 (*); $p < 0.001$ (**); $p = 0.001$ to 0.0001 (***) ; $p < 0.0001$ (****), ns = non-significant. The error bars indicate SD of the mean.

In severe cases of COVID-19, lung damage is a driving factor responsible for most patient fatalities⁴⁷ and diffuse alveolar damage (DAD) is a common histological finding in patients with severe COVID-19⁴⁸⁻⁵¹. DAD represents injury to type I pneumocytes or endothelial cells in the alveolar septa and is characterized by inflammation in the alveolus and alveolar septa and type II pneumocyte hyperplasia⁵²⁻⁵⁴. Although we observed no differences in composite lung pathology between lean and obese infected groups (Fig.3A & C), we did identify type II pneumocyte hyperplasia and inflammation of alveoli and alveolar septa in C57BL/6N and C3H/HeJ (Fig.4) mice, consistent with DAD, confirming the validity of our MHV-1 infection models for studying COVID-19 pathogenesis.

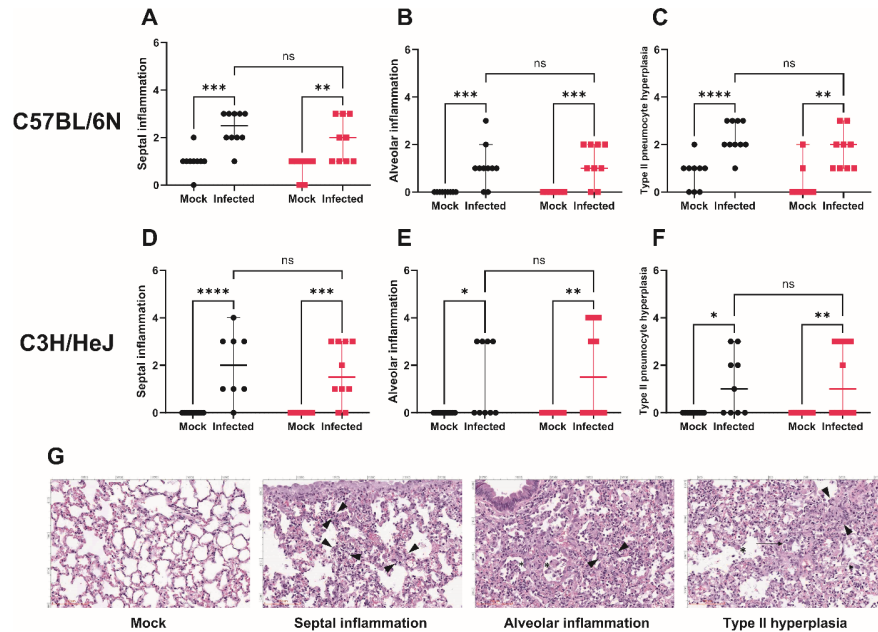


Fig.4: MHV-1 infection causes diffuse alveolar damage (DAD) in the lungs of C57BL/6N and C3H/HeJ mice.

Lungs of MHV-1 and mock-infected C3H/HeJ were collected for histopathological analysis. H&E-stained images were captured at 20X, scale bar = 100 μ m. Semi-quantitative histopathology scores showed significant inflammation of the septa and alveoli, along with the presence of type II pneumocyte hyperplasia, in MHV-1 infected compared to mock-infected C57BL/6N (A-C) and C3H/HeJ (D-F) mice. Statistical analysis was carried out by 2way ANOVA. **(G) Representative lung histopathology images from C3H/HeJ mice depicting diffuse alveolar lung damage (DAD).** Lungs of MHV-1 infected mice show alveolar and septal inflammation, along with type II pneumocyte hyperplasia compared to mock-infected mice. The level of significance is represented as follows: $p < 0.05$ (*); $p < 0.001$ (**); $p = 0.001$ to 0.0001 (***) ; $p < 0.0001$ (****), ns = non-significant. The error bars indicate SD of the mean.

Pathways and genes altered in obese C3H/HeJ mice exposed to MHV-1 are similar to those identified in severe COVID-19 patients. COVID-19 is a complex multisystem disorder involving vast interactions of immune and inflammatory pathways⁵⁵. Identifying potential disease-associated biomarkers may be useful to predict the outcome of COVID-19 in humans to assess risk levels to enable timely medical intervention. In this study, we hypothesized that blood would be an easily accessible clinical sample to monitor the complex transcriptional changes occurring early during the course of COVID-19. Therefore, we carried out RNAseq on blood from MHV-1 and mock-infected lean and obese C3H/HeJ mice at 2 dpi.

First, we carried out principal component analysis (PCA) to assess the clustering of the samples. We observed a clear separation between MHV-1 and mock-infected groups in lean and obese C3H/HeJ mice; in contrast, we observed no obvious clustering for lean and obese groups (Fig.5A), suggesting that infection, but not diet, contributes more significantly to gene expression changes between groups. Differential gene expression (DEG) analysis revealed 2635 upregulated and 863 downregulated genes in MHV-1 vs mock-infected lean mice (Supplementary Fig.S1-A) and 2089 upregulated and 681 downregulated genes in MHV-1 vs mock-infected obese mice (Supplementary Fig.S1-B). Pathway analysis was initially carried out by Gene Set Enrichment Analysis (GSEA) using Kyoto Encyclopedia of Genes and Genomes (KEGG) for identifying canonical pathways that were up or downregulated in MHV-1 infected vs mock lean (Supplementary Fig.S1-C) and obese mice (Supplementary Fig.S1-D). To account for the effect of mock infection on gene expression, we removed the genes expressed in mock-infected lean or obese mice from their MHV-1 infected counterparts and then identified unique DEGs in MHV-1 infected obese vs lean mice. There were 177 upregulated and 334 downregulated genes that were unique to MHV-1 infected obese mice compared to the infected lean mice, after adjusting for the DEG expression in their respective mocks and this list was used for generating pathways using the ShinyGO 0.77 analysis tool. These pathways were then compared to those identified in severe vs mild cases of COVID-19 (generated from data obtained from Wang et al.⁵⁶) and we found numerous upregulated (Fig.5B) and downregulated (Fig.5C) pathways shared between MHV-1 infected obese vs lean C3H/HeJ mice and human patients with severe vs mild COVID-19. The common upregulated pathways included Tumor necrosis factor (TNF) signaling, NOD-like receptor (NLR) signaling, platelet activation, Neutrophil extracellular trap (NET) formation, and Rap1 signaling pathways; while the common downregulated pathways included T cell receptor signaling pathway, Th1, Th2, Th17 cell-differentiation, inflammatory bowel disease, hematopoietic cell lineage, Natural Killer (NK) cell mediated cytotoxicity and primary immunodeficiency pathways.

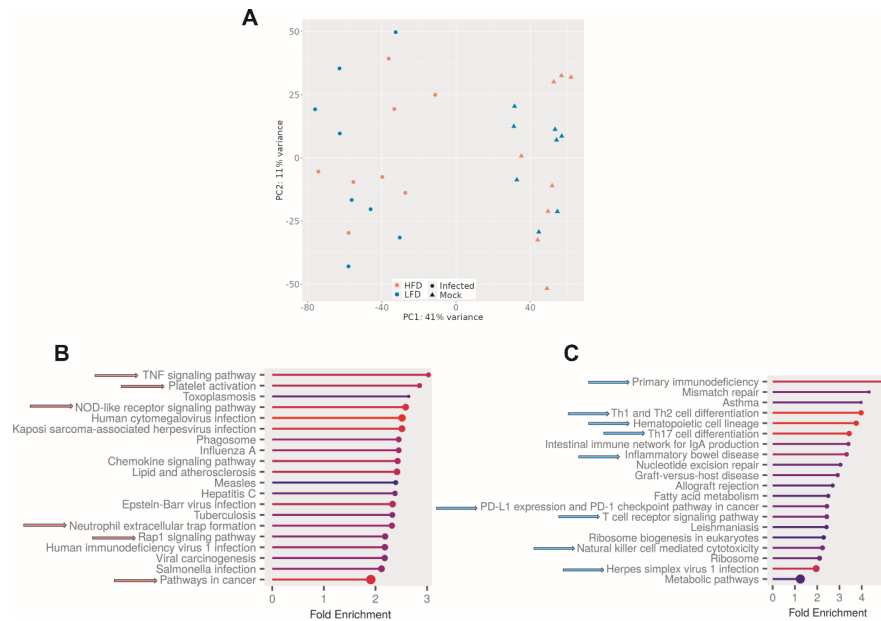


Fig.5: Similarities in gene expression and pathways in MHV-1 infected obese vs lean mice and severe vs mild COVID-19 patients.

RNAseq was performed on the RNA collected from blood of MHV-1 and mock-infected lean and obese C3H/HeJ mice (n = 8 per group) at 2 dpi. **(A) Principal component analysis (PCA) of MHV-1 and mock-infected lean and obese mice.** PC1 and PC2 were plotted to identify clustering of the MHV-1 and mock-infected samples. For identification of DEGs, genes with p-adjusted values < 0.1 and log₂FoldChange

> 1 , were selected by integrated Differential Expression and Pathway (iDEP .96) analysis tool. **Upregulated (B) and downregulated (C) pathways unique to MHV-1 infected obese vs lean mice.** For this comparison, gene expression in mock-infected lean or obese mice was removed from their MHV-1 infected counterparts and the resulting data was compared between obese and lean mice to identify DEGs unique to obese infected mice. For pathway analysis, DEGs with p-adjusted values < 0.1 and $\log_2\text{FoldChange} > 1$ were selected and pathways were generated using the ShinyGO 0.77 analysis tool. The pathways obtained were then compared to data from the blood of COVID-19 patients with severe disease; orange arrows indicate common upregulated and blue arrows indicate common downregulated pathways between MHV-1 infected obese vs lean mice and severe vs mild COVID-19 patients.

TNF has been shown to damage the respiratory epithelium and stimulate the synthesis of fibrin and collagen in the respiratory system^{57,58}. Although the direct role of TNF in severe COVID-19 has not yet been established, it has been associated with heart failure⁵⁹, blood clotting⁶⁰⁻⁶³, and is elevated in patients with obesity⁶⁴ and hypertension⁶⁵, all of which are risk factors for severe COVID-19. The NLR signaling pathway could potentially be linked to COVID-19 related multiple sclerosis (MS)⁶⁶ considering that the NLRP3 inflammasome has been implicated in COVID-19 pathogenesis⁶⁷. Platelet abnormalities in COVID-19 patients have been associated with disease severity and mortality⁶⁸ related to organ failure⁶⁹. The underlying mechanisms leading to severe COVID-19 symptoms, such as acute respiratory distress syndrome (ARDS), cytokine storm and thrombotic events, have been associated with neutrophils, particularly increased formation of neutrophil extracellular traps (NETs)⁷⁰. Excessive NET formation in SARS-CoV-2 infection has been associated with the onset of acute lung injury (ALI)⁷¹. The Rap1 signaling pathway has been implicated in the pathogenesis of respiratory, cardiovascular, and nervous system and some studies have shown that activation of the Rap1 signaling pathway can improve the symptoms of pulmonary fibrosis⁷².

T cells are recognized as potent immune modulators against various infections by activating cytotoxic or humoral immune-mediated reactions and are mainly divided into T helper type 1 (Th1), T helper type 2 (Th2), T helper type 17 (Th17) and regulatory T (Treg) cells⁷³. The equilibrium between Th1 and Th2 responses has been linked to COVID-19 outcomes, with an adequate Th1 response being associated with good prognosis and Th2 activation being linked to worse disease outcomes^{74,75}. Th17 has been associated with chronic inflammation and autoimmune diseases and may be involved in SARS-CoV-2 induced pneumonia⁷⁶. Similarly, the other downregulated pathways involved hematopoietic cell lineage, NK cell-mediated cytotoxicity and primary immunodeficiency, suggesting lowered lymphocyte immune responses in MHV-1-infected mice and COVID-19 patients.

We also compared expression of individual DEGs unique to MHV-1 infected obese vs. lean mice with expression patterns in severe vs mild COVID-19 patients and found 20 upregulated and 23 downregulated genes shared between MHV-1 and COVID-19 (Supplementary Table 1). In particular, MHV-1 infected obese mice exhibited upregulation of *B4galt5*⁷⁷, *Flt1*⁷⁸, *Stx3*⁷⁹, and *Ass1*⁸⁰ and downregulation of *Crip2*⁷⁷ and *Rora*⁸¹ changes (Supplementary Fig.S2) which have also been associated with severe disease outcomes in COVID-19 patients. Strikingly, the similarities observed in the immune pathways and gene expression patterns in our MHV-1 infected obese vs lean mice suggest that our coronavirus infection model mimics COVID-19 in humans and could be a potentially relevant model to identify biomarkers of severe disease outcome in SARS-CoV-2 infected individuals. However, future mechanistic studies are needed to elucidate the precise roles of these biomarkers in coronavirus disease outcomes.

Gene Set Variation Analysis (GSVA) showed significant differences between MHV-1 infected lean and obese C3H/HeJ mice. We further utilized our RNAseq data to carry out Gene Set Variation Analysis (GSVA) and compare the impact of MHV-1 infection and obesity on differential enrichment of disease-relevant immune cell, inflammatory, and cellular pathway gene signatures^{12,33,82} (Fig.6A & B). Several immune cell type signatures associated with COVID-19 patient disease pathology were also changed in MHV-1 infected mice, including enrichment of inflammatory neutrophils, low density granulocytes (LDGs), monocytes, and activated B cells as well as de-enrichment of T cells (Fig.6A). Pathway gene signatures representing response to inflammatory cytokines, such as interferons (IFN) and TNF, as well as metabolic

pathways, including glycolysis and lipid metabolism were also elevated in infected mice (Fig.6B). Gene expression changes associated with obesity in the context of infection were much more subtle. However, we did find that the unfolded protein and lipid metabolism gene signatures were significantly increased suggesting that dysregulated cell stress and metabolism pathways could be involved in exacerbating disease outcomes in obese mice (Fig.6B).

In order to relate disease pathology with changes in gene expression, we carried out linear regression analysis using the inflammatory neutrophil gene signature, which was derived from gene expression studies of severe COVID-19 patients⁸³, and clinical features. This revealed a significant correlation between the inflammatory neutrophil GSVA enrichment score and weight loss as well as lung and liver tissue pathology scores (Fig.6C-E) suggesting inflammatory neutrophils may also be contributing to disease severity in MHV-1 infected mice. In contrast, the activated B cell gene signature was significantly correlated with overall weight loss (Fig.6F), but not tissue pathology scores (Fig.6G-H) indicating that inflammatory neutrophils and not B cells were associated with tissue damage in infected mice. Overall, we have demonstrated the utility of MHV-1 infected C3H/HeJ mice as a model for human COVID-19 as well as the effect of diet-induced obesity on disease pathogenesis.

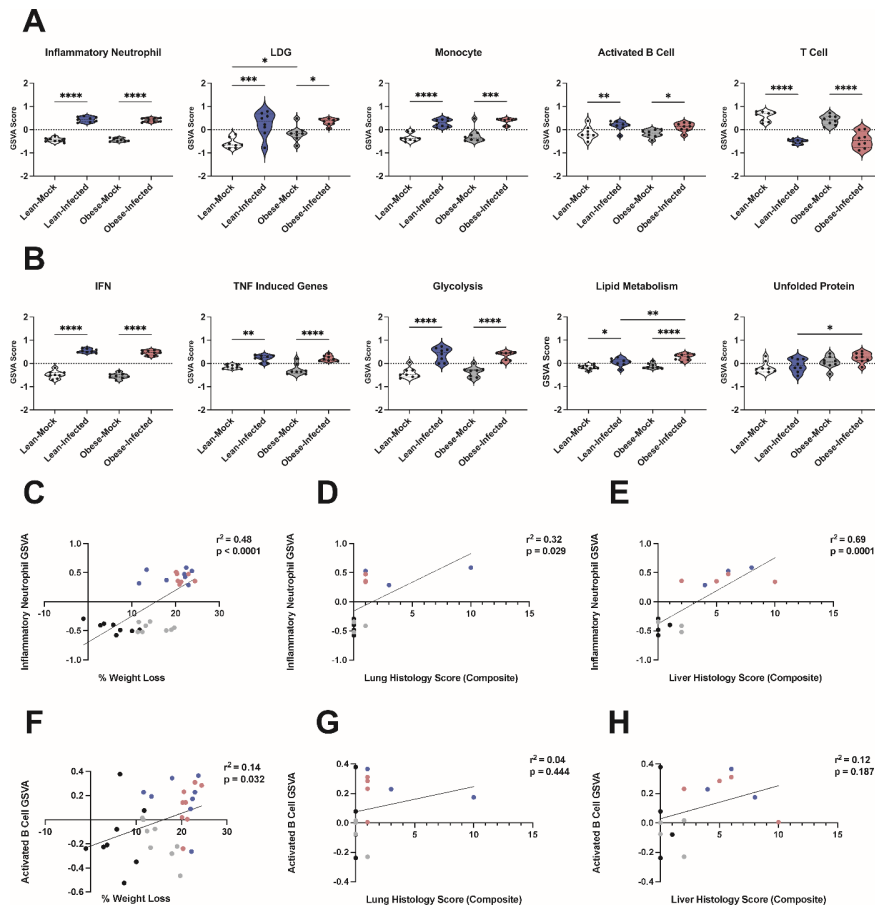


Fig.6: GSVA showed significant correlation between inflammatory neutrophils and measures of disease severity.

RNAseq data from MHV-1 and mock-infected lean and obese C3H/HeJ mice was analyzed by GSVA using immune cell (A) and inflammatory and cellular pathway (B) gene signatures.

Linear regression analysis between inflammatory neutrophil GSVA scores and weight loss (C), lung histopathology (D) and liver histopathology (E). Linear regression analysis between activated B cell GSVA scores and weight loss (F), lung histopathology (G) and liver histopathology (H). The correlation for each comparison is displayed as the r^2 value and the significance of the correlation is displayed as the p-value. Statistical and regression analysis was done using GraphPad Prism. The level of significance is represented as follows: $p < 0.05$ (*); $p < 0.001$ (**); $p = 0.001$ to 0.0001 (***) ; $p < 0.0001$ (****). The error bars indicate SD of the mean.

Conclusions

In summary, we have identified a relevant mouse model that mimics COVID-19 in humans. We have leveraged this model to explore the complex relationship between obesity and coronavirus disease severity. Our findings suggest that obesity contributes to increased susceptibility to severe coronavirus disease and may modulate tissue-specific responses. Moreover, the identification of potential biomarkers shared with severe COVID-19 cases in humans can be utilized to forecast disease outcomes, assess risk levels, and prognose high-risk patients to enable timely medical intervention. Future mechanistic studies are needed to elucidate the precise roles of these biomarkers in coronavirus disease outcomes.

Supplementary Figures

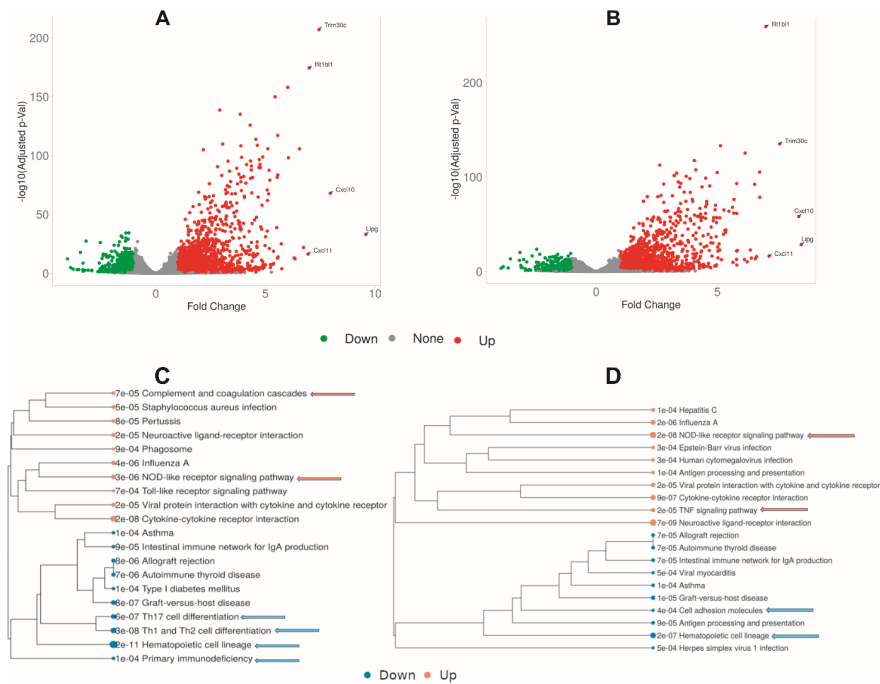


Fig.S1: Differential gene expression and pathway analysis in MHV-1 vs mock-infected lean and obese C3H/HeJ mice.

RNAseq was performed on the RNA collected from blood of MHV-1 and mock-infected lean and obese C3H/HeJ mice at 2 dpi. **(A & B) Volcano plot of differentially expressed genes (DEGs) for lean (A) and obese (B) mice.** For identification of DEGs, genes with p -adjusted values < 0.1 and $\log_2\text{FoldChange} > 1$, were selected by integrated Differential Expression and Pathway (iDEP .96) analysis tool. **(C & D) Pathway analysis for lean (C) and obese (D) mice.** Pathways were generated using Gene Set Enrichment Analysis (GSEA) using the Kyoto Encyclopedia of Genes and Genomes (KEGG). All the pathway analysis data were compared to data from the blood of COVID-19 patients with severe disease;

orange arrows indicate common upregulated and blue arrows indicate common downregulated pathways between MHV-1 infected vs mock and severe vs mild COVID-19 patients and the common up or downregulated pathways are represented by arrows.

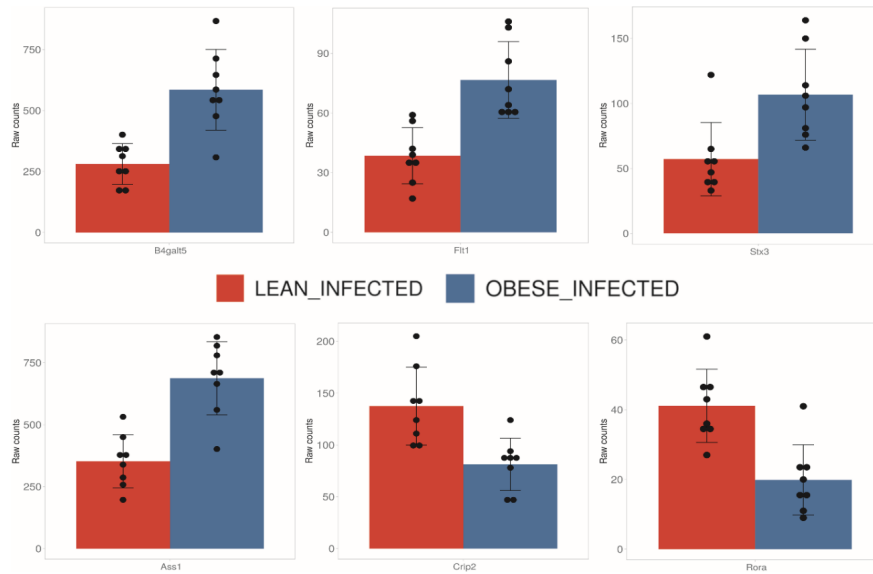


Fig.S2: Expression patterns of genes in MHV-1 infected obese vs lean C3H/HeJ mice, based on raw counts data.

Biomarker genes were identified after comparing the mouse RNAseq data to severe vs mild COVID-19 patient data. Then iDEP 2.0 was used to perform gene plots on raw counts, with standard deviation, for the identified genes between MHV-1 infected obese and lean mice. B4galt5, Flt1, Stx3 and Ass1 showed a trend towards upregulation, while Crp2 and Rora showed a trend towards downregulation in obese vs lean mice.

Supplementary Tables

Supplementary Table 1. List of up and downregulated DEGs, with \log_2 Fold Change values, unique to MHV-1 infected obese vs lean C3H/HeJ mice with similar expression as severe vs mild COVID-19 patients.

Symbol	Log ₂ Fold Change	Log ₂ Fold Change	Regulation
	MHV-1	COVID-19	
Srgap1	5.593313745	1.288614	Up
Scn2b	4.760590346	0.8709768	Up
Hmcn1	4.674269052	0.77173757	Up
Lvrn	4.525300694	0.9098423	Up
Flt1	4.464887932	1.431504705	Up
Ticrr	3.146043378	1.533416	Up
Pdss1	1.891486116	0.6600827	Up
Pole2	1.725676487	0.7632403	Up
Arhgef37	1.697521173	1.362466202	Up
Myo10	1.640562322	1.429666	Up
Cc2d2b	1.45096369	1.862170706	Up
B4galt5	1.383974831	1.306495789	Up
Dnajc13	1.357049965	0.607348669	Up

Symbol	Log ₂ Fold Change	Log ₂ Fold Change	Regulation
Stx3	1.327024085	0.9542184	Up
Asph	1.283336276	2.192180081	Up
Ass1	1.174287366	0.665236365	Up
Slc8a1	1.069356564	1.531484	Up
Esam	1.046268861	1.319889762	Up
Tifa	1.044719796	0.8567695	Up
Trim9	1.348867313	1.061524	Up
Dtx3	-1.142670519	-1.290120726	Down
Kif3a	-1.100795517	-0.9768302	Down
Matk	-1.17576259	-1.677993	Down
Cdc25b	-1.366412368	-1.033647957	Down
Crip2	-1.246176575	-1.189354949	Down
Rora	-1.106910332	-1.600963	Down
Sh3y11	-1.380657957	-0.7296559	Down
Kctd7	-1.243119704	-0.6274643	Down
Clic3	-2.546052451	-1.657180512	Down
Ctsf	-1.376541686	-0.830037696	Down
St8sia6	-1.070073644	-0.8505567	Down
Igsf8	-1.038611817	-0.8450607	Down
Egr2	-2.209850344	-0.776069905	Down
Syng1	-1.115853608	-0.7681419	Down
Ddb2	-1.397359623	-0.743174555	Down
Hspa12a	-2.842163756	-0.699411	Down
Akap7	-1.094982427	-0.65468549	Down
Zfp1	-1.569822542	-0.6469833	Down
Dusp8	-1.667002083	-0.624085255	Down
Reep6	-1.715118998	-0.6239955	Down
Pkd11l1	-1.611257667	-0.6195963	Down
Plxnd1	-1.196410739	-0.6095316	Down
Mars2	-1.332546191	-0.5980099	Down

Supplementary Table 2. Gene sets used as input for GSVA.

Gene Symbol	Entrez ID	Gene Set
Ada	11486	Activated B Cell
Batf	53314	Activated B Cell
Bcl3	12051	Activated B Cell
Cd28	12487	Activated B Cell
Cd69	12515	Activated B Cell
Cd80	12519	Activated B Cell
Cd86	12524	Activated B Cell
Mad2l2	71890	Activated B Cell
Nans	94181	Activated B Cell
Slc3a2	17254	Activated B Cell
Ung	22256	Activated B Cell
Xrcc4	108138	Activated B Cell
Aldoa	11674	Glycolysis
Aldob	230163	Glycolysis
Aldoc	11676	Glycolysis

Gene Symbol	Entrez ID	Gene Set
Eno1	13806	Glycolysis
Gpi1	14751	Glycolysis
Hk2	15277	Glycolysis
Hkdc1	216019	Glycolysis
Ldha	16828	Glycolysis
Pfkfb3	170768	Glycolysis
Pfkp	56421	Glycolysis
Pgk1	18655	Glycolysis
Pkm	18746	Glycolysis
Slc2a1	20525	Glycolysis
Tpi1	21991	Glycolysis
Eif2ak2	19106	IFN
Gbp2	14469	IFN
Gbp3	55932	IFN
Herc6	67138	IFN
Ifi27	52668	IFN
Ifi30	65972	IFN
Ifi35	70110	IFN
Ifi44	99899	IFN
Ifi44l	15061	IFN
Ifit1	15957	IFN
Ifit2	15958	IFN
Ifit3	15959	IFN
Ifitm1	68713	IFN
Ifitm2	80876	IFN
Ifitm3	66141	IFN
Isg15	100038882	IFN
Isg20	57444	IFN
Mx1	17857	IFN
Mx2	17858	IFN
Oas1a	246730	IFN
Oas2	246728	IFN
Oas3	246727	IFN
Oasl1	231655	IFN
Rsad2	58185	IFN
Sp100	20684	IFN
Sp110	109032	IFN
1810037I17Rik	67704	Inflammatory_Neutrophil
Acs1l	14081	Inflammatory_Neutrophil
Adar	56417	Inflammatory_Neutrophil
Add3	27360	Inflammatory_Neutrophil
Adm	11535	Inflammatory_Neutrophil
Alox5ap	11690	Inflammatory_Neutrophil
Alpl	11647	Inflammatory_Neutrophil
Anxa1	16952	Inflammatory_Neutrophil
Anxa3	11745	Inflammatory_Neutrophil
Apol6	71939	Inflammatory_Neutrophil
Apol8	239552	Inflammatory_Neutrophil
B4galt5	56336	Inflammatory_Neutrophil
Baz1a	217578	Inflammatory_Neutrophil

Gene Symbol	Entrez ID	Gene Set
Bri3	55950	Inflammatory_Neutrophil
Bst1	12182	Inflammatory_Neutrophil
C3ar1	12267	Inflammatory_Neutrophil
Capza1	12340	Inflammatory_Neutrophil
Casp1	12362	Inflammatory_Neutrophil
Casp1	12362	Inflammatory_Neutrophil
Casp4	12363	Inflammatory_Neutrophil
Cast	12380	Inflammatory_Neutrophil
Ccr1	12768	Inflammatory_Neutrophil
Cd177	68891	Inflammatory_Neutrophil
Cd37	12493	Inflammatory_Neutrophil
Cd44	12505	Inflammatory_Neutrophil
Cd53	12508	Inflammatory_Neutrophil
Cd55	13136	Inflammatory_Neutrophil
Cd55b	13137	Inflammatory_Neutrophil
Cd63	12512	Inflammatory_Neutrophil
Cd82	12521	Inflammatory_Neutrophil
Cdkn2d	12581	Inflammatory_Neutrophil
Ceacam1	26365	Inflammatory_Neutrophil
Cfl1	12631	Inflammatory_Neutrophil
Ckap4	216197	Inflammatory_Neutrophil
Clec4d	17474	Inflammatory_Neutrophil
Clec4e	56619	Inflammatory_Neutrophil
Cr11	12946	Inflammatory_Neutrophil
Cst7	13011	Inflammatory_Neutrophil
Cystm1	66060	Inflammatory_Neutrophil
Ddx60	234311	Inflammatory_Neutrophil
Dysf	26903	Inflammatory_Neutrophil
Eif2ak2	19106	Inflammatory_Neutrophil
Emb	13723	Inflammatory_Neutrophil
Epsti1	108670	Inflammatory_Neutrophil
Fcer1g	14127	Inflammatory_Neutrophil
Fcgr1	14129	Inflammatory_Neutrophil
Ffar2	233079	Inflammatory_Neutrophil
Fgr	14191	Inflammatory_Neutrophil
Fkbp1a	14225	Inflammatory_Neutrophil
Fkbp5	14229	Inflammatory_Neutrophil
Flot1	14251	Inflammatory_Neutrophil
Fyb	23880	Inflammatory_Neutrophil
Gapdh	14433	Inflammatory_Neutrophil
Gbp2	14469	Inflammatory_Neutrophil
Gbp3	55932	Inflammatory_Neutrophil
Gbp5	229898	Inflammatory_Neutrophil
Gca	227960	Inflammatory_Neutrophil
Gimap4	107526	Inflammatory_Neutrophil
Glrx	93692	Inflammatory_Neutrophil
Gng5	14707	Inflammatory_Neutrophil
Grina	66168	Inflammatory_Neutrophil
Grn	14824	Inflammatory_Neutrophil
Gstk1	76263	Inflammatory_Neutrophil

Gene Symbol	Entrez ID	Gene Set
Gyg	27357	Inflammatory_Neutrophil
H2-M3	14991	Inflammatory_Neutrophil
H2-Q1	15006	Inflammatory_Neutrophil
H2-Q2	15013	Inflammatory_Neutrophil
H2ac1	319163	Inflammatory_Neutrophil
H2ac23	665433	Inflammatory_Neutrophil
H2bc14	319186	Inflammatory_Neutrophil
Hif1a	15251	Inflammatory_Neutrophil
Hmgb2	97165	Inflammatory_Neutrophil
I830077J02Rik	433638	Inflammatory_Neutrophil
Ifi205	226695	Inflammatory_Neutrophil
Ifi44	99899	Inflammatory_Neutrophil
Ifi44l	15061	Inflammatory_Neutrophil
Ifih1	71586	Inflammatory_Neutrophil
Ifit1b1l	667373	Inflammatory_Neutrophil
Ifit2	15958	Inflammatory_Neutrophil
Ifit3	15959	Inflammatory_Neutrophil
Ifitm1	68713	Inflammatory_Neutrophil
Ifitm3	66141	Inflammatory_Neutrophil
Il1rn	16181	Inflammatory_Neutrophil
Il2rg	16186	Inflammatory_Neutrophil
Irf1	16362	Inflammatory_Neutrophil
Irf7	54123	Inflammatory_Neutrophil
Isg15	100038882	Inflammatory_Neutrophil
Isg20	57444	Inflammatory_Neutrophil
Itgam	16409	Inflammatory_Neutrophil
Jun	16476	Inflammatory_Neutrophil
Kcnj15	16516	Inflammatory_Neutrophil
Klf4	16600	Inflammatory_Neutrophil
Lap3	66988	Inflammatory_Neutrophil
Lgals9	16859	Inflammatory_Neutrophil
Lilra5	232801	Inflammatory_Neutrophil
Lilra6	18726	Inflammatory_Neutrophil
Limk2	16886	Inflammatory_Neutrophil
Lmnb1	16906	Inflammatory_Neutrophil
Lrg1	76905	Inflammatory_Neutrophil
Ly6e	17069	Inflammatory_Neutrophil
Ly96	17087	Inflammatory_Neutrophil
Mapk14	26416	Inflammatory_Neutrophil
Max	17187	Inflammatory_Neutrophil
Mcemp1	69189	Inflammatory_Neutrophil
Mettl9	59052	Inflammatory_Neutrophil
Mmp9	17395	Inflammatory_Neutrophil
Mob1a	232157	Inflammatory_Neutrophil
Msrb1	27361	Inflammatory_Neutrophil
Mt2	17750	Inflammatory_Neutrophil
Mtpn	14489	Inflammatory_Neutrophil
Mx2	17858	Inflammatory_Neutrophil
Myl12a	67268	Inflammatory_Neutrophil
Nbn	27354	Inflammatory_Neutrophil

Gene Symbol	Entrez ID	Gene Set
Nfe2	18022	Inflammatory_Neutrophil
Nfil3	18030	Inflammatory_Neutrophil
Nfkbia	18035	Inflammatory_Neutrophil
Nmi	64685	Inflammatory_Neutrophil
Nt5c3	107569	Inflammatory_Neutrophil
Ntng2	171171	Inflammatory_Neutrophil
Nub1	53312	Inflammatory_Neutrophil
Nucb1	18220	Inflammatory_Neutrophil
Oas1a	246730	Inflammatory_Neutrophil
Oas1g	23960	Inflammatory_Neutrophil
Oas2	246728	Inflammatory_Neutrophil
Oas3	246727	Inflammatory_Neutrophil
Oasl1	231655	Inflammatory_Neutrophil
Parp14	547253	Inflammatory_Neutrophil
Parp9	80285	Inflammatory_Neutrophil
Pgd	110208	Inflammatory_Neutrophil
Phf11a	219131	Inflammatory_Neutrophil
Phf11b	236451	Inflammatory_Neutrophil
Phf11d	219132	Inflammatory_Neutrophil
Pik3ap1	83490	Inflammatory_Neutrophil
Pim1	18712	Inflammatory_Neutrophil
Pira12	100038909	Inflammatory_Neutrophil
Pira13	100041146	Inflammatory_Neutrophil
Pira2	18725	Inflammatory_Neutrophil
Pirb	18733	Inflammatory_Neutrophil
Plac8	231507	Inflammatory_Neutrophil
Plbd1	66857	Inflammatory_Neutrophil
Plek	56193	Inflammatory_Neutrophil
Plp2	18824	Inflammatory_Neutrophil
Plscr1	22038	Inflammatory_Neutrophil
Pml	18854	Inflammatory_Neutrophil
Prok2	50501	Inflammatory_Neutrophil
Prr13	66151	Inflammatory_Neutrophil
Psmb9	16912	Inflammatory_Neutrophil
Pstpip2	19201	Inflammatory_Neutrophil
Pten	19211	Inflammatory_Neutrophil
Rac2	19354	Inflammatory_Neutrophil
Rbck1	24105	Inflammatory_Neutrophil
Rbms1	56878	Inflammatory_Neutrophil
Rgs19	56470	Inflammatory_Neutrophil
Rhog	56212	Inflammatory_Neutrophil
Rnf10	50849	Inflammatory_Neutrophil
Rnf213	672511	Inflammatory_Neutrophil
Rpl28	19943	Inflammatory_Neutrophil
Rsad2	58185	Inflammatory_Neutrophil
S100a6	20200	Inflammatory_Neutrophil
Samd9l	209086	Inflammatory_Neutrophil
Samhd1	56045	Inflammatory_Neutrophil
Samsn1	67742	Inflammatory_Neutrophil
Sat1	20229	Inflammatory_Neutrophil

Gene Symbol	Entrez ID	Gene Set
Sectm1a	209588	Inflammatory_Neutrophil
Sell	20343	Inflammatory_Neutrophil
Serpina1b	20701	Inflammatory_Neutrophil
Serpina1e	20704	Inflammatory_Neutrophil
Serpina1a	66222	Inflammatory_Neutrophil
Serping1	12258	Inflammatory_Neutrophil
Sh3glb1	54673	Inflammatory_Neutrophil
Shisa5	66940	Inflammatory_Neutrophil
Slfn5	327978	Inflammatory_Neutrophil
Snx3	54198	Inflammatory_Neutrophil
Sp100	20684	Inflammatory_Neutrophil
Sp110	109032	Inflammatory_Neutrophil
Spi1	20375	Inflammatory_Neutrophil
Sptlc2	20773	Inflammatory_Neutrophil
Stat1	20846	Inflammatory_Neutrophil
Stat2	20847	Inflammatory_Neutrophil
Stxbp2	20911	Inflammatory_Neutrophil
Tap1	21354	Inflammatory_Neutrophil
Tmem123	71929	Inflammatory_Neutrophil
Tmsb10	19240	Inflammatory_Neutrophil
Tnfaip6	21930	Inflammatory_Neutrophil
Tnfsf10	22035	Inflammatory_Neutrophil
Tnfsf13b	24099	Inflammatory_Neutrophil
Tpm3	59069	Inflammatory_Neutrophil
Trim38	214158	Inflammatory_Neutrophil
Txn1	22166	Inflammatory_Neutrophil
Ube2j1	56228	Inflammatory_Neutrophil
Ube2l6	56791	Inflammatory_Neutrophil
Vim	22352	Inflammatory_Neutrophil
Wsb1	78889	Inflammatory_Neutrophil
Xaf1	327959	Inflammatory_Neutrophil
Xrn1	24127	Inflammatory_Neutrophil
Zbp1	58203	Inflammatory_Neutrophil
Zcchc2	227449	Inflammatory_Neutrophil
Zdhhc19	245308	Inflammatory_Neutrophil
Zyx	22793	Inflammatory_Neutrophil
Ctsg	13035	LDG
Elane	50701	LDG
Lcn2	16819	LDG
Mpo	17523	LDG
Osm	18413	LDG
Aadac	67758	Lipid Metabolism
Abhd6	6082	Lipid Metabolism
Acly	104112	Lipid Metabolism
Acsl5	433256	Lipid Metabolism
Angptl3	30924	Lipid Metabolism
Angptl4	57875	Lipid Metabolism
Apoa4	11808	Lipid Metabolism
Apoa5	66113	Lipid Metabolism
Apoe	11816	Lipid Metabolism

Gene Symbol	Entrez ID	Gene Set
Apoh	11818	Lipid Metabolism
Ccdc3	74186	Lipid Metabolism
Cnep1r1	382030	Lipid Metabolism
Dbi	13167	Lipid Metabolism
Dgat1	13350	Lipid Metabolism
Dgat2	67800	Lipid Metabolism
Disp3	242748	Lipid Metabolism
Fabp3	14077	Lipid Metabolism
Gpam	14732	Lipid Metabolism
Gpld1	14756	Lipid Metabolism
Hsd17b13	243168	Lipid Metabolism
Ldlr	16835	Lipid Metabolism
Mid1ip1	68041	Lipid Metabolism
Nr1h2	22260	Lipid Metabolism
Nr1h3	22259	Lipid Metabolism
Pcx	18563	Lipid Metabolism
Pnpla2	66853	Lipid Metabolism
Ppara	19013	Lipid Metabolism
Slc27a1	26457	Lipid Metabolism
Srebfl	20787	Lipid Metabolism
Bst1	12182	Monocyte
C1qa	12259	Monocyte
C1qb	12260	Monocyte
C1qc	12262	Monocyte
C1rl	232371	Monocyte
Ccl8	20307	Monocyte
Cd14	12475	Monocyte
Cd163	93671	Monocyte
Cd68	12514	Monocyte
Clec10a	17312	Monocyte
Clec12a	232413	Monocyte
Clec4d	17474	Monocyte
Clec4e	56619	Monocyte
Csf1r	12978	Monocyte
Cxcl1	14825	Monocyte
Cxcl10	15945	Monocyte
Fcgr1	14129	Monocyte
Fcgr4	246256	Monocyte
Ifi211	381308	Monocyte
Il1b	16176	Monocyte
Il1rn	16181	Monocyte
Lilra5	232801	Monocyte
Mrc1	17533	Monocyte
Oscar	232790	Monocyte
P2rx5	94045	Monocyte
Pirb	18733	Monocyte
Sema4a	20351	Monocyte
Siglec1	20612	Monocyte
Thbd	21824	Monocyte
Tnf	21926	Monocyte

Gene Symbol	Entrez ID	Gene Set
Cd247	12503	T Cell
Cd28	12487	T Cell
Cd3d	12500	T Cell
Cd3e	12501	T Cell
Cd3g	12502	T Cell
Cd4	12504	T Cell
Cd5	12507	T Cell
Cd8a	12525	T Cell
Cd8b1	12526	T Cell
Ets1	23871	T Cell
Gata3	14462	T Cell
Grap2	17444	T Cell
Lef1	16842	T Cell
Sh2d1a	20400	T Cell
Trac	100101484	T Cell
Trbc1	100125262	T Cell
TRDC	100123473	T Cell
Bcl2l10	12049	TNF Induced Genes
Ccl5	20304	TNF Induced Genes
Cd6	12511	TNF Induced Genes
Cd68	12514	TNF Induced Genes
Cp	12870	TNF Induced Genes
Csf2	12981	TNF Induced Genes
Csf3	12985	TNF Induced Genes
Dcn	13179	TNF Induced Genes
Gbp2	14469	TNF Induced Genes
Gdf15	23886	TNF Induced Genes
Gstt1	14871	TNF Induced Genes
H2-D1	14964	TNF Induced Genes
H2-K2	630499	TNF Induced Genes
H2-T23	15040	TNF Induced Genes
Hp	15439	TNF Induced Genes
Igdcc3	19289	TNF Induced Genes
Il6	16193	TNF Induced Genes
Jun	16476	TNF Induced Genes
Krt35	53617	TNF Induced Genes
Limk1	16885	TNF Induced Genes
Madcam1	17123	TNF Induced Genes
Mmp13	17386	TNF Induced Genes
Mmp3	17392	TNF Induced Genes
Nfkbia	18035	TNF Induced Genes
Notch3	18131	TNF Induced Genes
Saa3	20210	TNF Induced Genes
Sele	20339	TNF Induced Genes
Selp	20344	TNF Induced Genes
Serpina3n	20716	TNF Induced Genes
Sod2	20656	TNF Induced Genes
Tap2	21355	TNF Induced Genes
Tnfaip3	21929	TNF Induced Genes
Traf1	22029	TNF Induced Genes

Gene Symbol	Entrez ID	Gene Set
Vcam1	22329	TNF Induced Genes
Yy1	22632	TNF Induced Genes
Bpnt2	242291	Unfolded Protein
Calr	12317	Unfolded Protein
Calu	12321	Unfolded Protein
Canx	12330	Unfolded Protein
Cds2	110911	Unfolded Protein
Der11	67819	Unfolded Protein
Der12	116891	Unfolded Protein
Dnajc3	100037258	Unfolded Protein
Edem2	108687	Unfolded Protein
Edem3	66967	Unfolded Protein
Erap1	80898	Unfolded Protein
Ergic2	67456	Unfolded Protein
Ero11	50527	Unfolded Protein
Ext1	14042	Unfolded Protein
Galnt2	108148	Unfolded Protein
Golt1b	66964	Unfolded Protein
Herpud1	64209	Unfolded Protein
Hyou1	12282	Unfolded Protein
Kdelr2	66913	Unfolded Protein
Lman2	66890	Unfolded Protein
Lpgat1	226856	Unfolded Protein
Man1a	17155	Unfolded Protein
Manea	242362	Unfolded Protein
Manf	74840	Unfolded Protein
Pdia4	12304	Unfolded Protein
Pdia6	71853	Unfolded Protein
Pigk	329777	Unfolded Protein
Poglut2	72050	Unfolded Protein
Ppib	19035	Unfolded Protein
Sec24d	69608	Unfolded Protein
Sec61g	20335	Unfolded Protein
Spcs3	76687	Unfolded Protein
Ssr1	107513	Unfolded Protein
Ssr3	67437	Unfolded Protein
Tram1	72265	Unfolded Protein
Tram2	170829	Unfolded Protein
Uggt1	320011	Unfolded Protein
Xbp1	22433	Unfolded Protein

References

1. Abdool Karim SS, de Oliveira T. New SARS-CoV-2 Variants — Clinical, Public Health, and Vaccine Implications. *New England Journal of Medicine* . 2021;384(19):1866-1868. doi:10.1056/NEJMc2100362
2. Aydogdu MO, Rohn JL, Jafari NV, Brako F, Homer-Vanniasinkam S, Edirisinghe M. Severe Acute Respiratory Syndrome Type 2-Causing Coronavirus: Variants and Preventive Strategies. *Adv Sci (Weinh)* . Apr 2022;9(11):e2104495. doi:10.1002/advs.202104495
3. WHO. WHO Coronavirus (COVID-19) Dashboard. *WHO* . 09/13/2023 2023;

4. Robba C, Battaglini D, Pelosi P, Rocco PRM. Multiple organ dysfunction in SARS-CoV-2: MODS-CoV-2. *Expert Review of Respiratory Medicine* . 2020/09/01 2020;14(9):865-868. doi:10.1080/17476348.2020.1778470
5. Kruglikov IL, Shah M, Scherer PE. Obesity and diabetes as comorbidities for COVID-19: Underlying mechanisms and the role of viral-bacterial interactions. *Elife* . Sep 15 2020;9doi:10.7554/eLife.61330
6. Liu Z, Li J, Huang J, et al. Association Between Diabetes and COVID-19: A Retrospective Observational Study With a Large Sample of 1,880 Cases in Leishenshan Hospital, Wuhan. *Front Endocrinol (Lausanne)* . 2020;11:478. doi:10.3389/fendo.2020.00478
7. Caussy C, Wallet F, Laville M, Disse E. Obesity is associated with severe forms of COVID-19. *Obesity* . 2020;28(7):1175-1175.
8. Deng M, Qi Y, Deng L, et al. Obesity as a potential predictor of disease severity in young COVID-19 patients: a retrospective study. *Obesity* . 2020;28(10):1815-1825.
9. Richardson S, Hirsch JS, Narasimhan M, et al. Presenting Characteristics, Comorbidities, and Outcomes Among 5700 Patients Hospitalized With COVID-19 in the New York City Area. *Jama* . May 26 2020;323(20):2052-2059. doi:10.1001/jama.2020.6775
10. Singh AK, Gupta R, Misra A. Comorbidities in COVID-19: Outcomes in hypertensive cohort and controversies with renin angiotensin system blockers. *Diabetes Metab Syndr* . Jul-Aug 2020;14(4):283-287. doi:10.1016/j.dsx.2020.03.016
11. Zhang F, Xiong Y, Wei Y, et al. Obesity predisposes to the risk of higher mortality in young COVID-19 patients. *J Med Virol* . Nov 2020;92(11):2536-2542. doi:10.1002/jmv.26039
12. Daamen AR, Bachali P, Owen KA, et al. Comprehensive transcriptomic analysis of COVID-19 blood, lung, and airway. *Sci Rep* . Mar 29 2021;11(1):7052. doi:10.1038/s41598-021-86002-x
13. Giamarellos-Bourboulis EJ, Netea MG, Rovina N, et al. Complex Immune Dysregulation in COVID-19 Patients with Severe Respiratory Failure. *Cell Host Microbe* . Jun 10 2020;27(6):992-1000.e3. doi:10.1016/j.chom.2020.04.009
14. Sattar N, McInnes IB, McMurray JJV. Obesity Is a Risk Factor for Severe COVID-19 Infection: Multiple Potential Mechanisms. *Circulation* . Jul 7 2020;142(1):4-6. doi:10.1161/circulationaha.120.047659
15. Rottoli M, Bernante P, Belvedere A, et al. How important is obesity as a risk factor for respiratory failure, intensive care admission and death in hospitalised COVID-19 patients? Results from a single Italian centre. *Eur J Endocrinol* . Oct 2020;183(4):389-397. doi:10.1530/eje-20-0541
16. Syed AA, Soran H, Adam S. Obesity and covid-19: the unseen risks. *Bmj* . Jul 16 2020;370:m2823. doi:10.1136/bmj.m2823
17. Lighter J, Phillips M, Hochman S, et al. Obesity in Patients Younger Than 60 Years Is a Risk Factor for COVID-19 Hospital Admission. *Clin Infect Dis* . Jul 28 2020;71(15):896-897. doi:10.1093/cid/ciaa415
18. Deng M, Qi Y, Deng L, et al. Obesity as a Potential Predictor of Disease Severity in Young COVID-19 Patients: A Retrospective Study. *Obesity (Silver Spring)* . Oct 2020;28(10):1815-1825. doi:10.1002/oby.22943
19. Bantulà M, Tubita V, Roca-Ferrer J, et al. Differences in Inflammatory Cytokine Profile in Obesity-Associated Asthma: Effects of Weight Loss. *J Clin Med* . Jun 29 2022;11(13)doi:10.3390/jcm11133782
20. Khanna D, Khanna S, Khanna P, Kahar P, Patel BM. Obesity: A Chronic Low-Grade Inflammation and Its Markers. *Cureus* . Feb 2022;14(2):e22711. doi:10.7759/cureus.22711
21. Lee KS, Russ BP, Wong TY, et al. Diet induced obesity and type 2 diabetes drives exacerbated sex-associated disease profiles in K18-hACE2-mice challenged with SARS-CoV-2. *bioRxiv* . 2022:2022.04.26.489580. doi:10.1101/2022.04.26.489580

22. Zhang Y-N, Zhang Z-R, Zhang H-Q, et al. Increased morbidity of obese mice infected with mouse-adapted SARS-CoV-2. *Cell Discovery* . 2021/08/25 2021;7(1):74. doi:10.1038/s41421-021-00305-x
23. Khanolkar A, Hartwig SM, Haag BA, et al. Protective and pathologic roles of the immune response to mouse hepatitis virus type 1: implications for severe acute respiratory syndrome. *J Virol* . Sep 2009;83(18):9258-72. doi:10.1128/jvi.00355-09
24. Khanolkar A, Hartwig SM, Haag BA, Meyerholz DK, Harty JT, Varga SM. Toll-Like Receptor 4 Deficiency Increases Disease and Mortality after Mouse Hepatitis Virus Type 1 Infection of Susceptible C3H Mice. *Journal of Virology* . 2009;83(17):8946-8956. doi:10.1128/jvi.01857-08
25. Khanolkar A, Fulton RB, Epping LL, et al. T cell epitope specificity and pathogenesis of mouse hepatitis virus-1-induced disease in susceptible and resistant hosts. *J Immunol* . Jul 15 2010;185(2):1132-41. doi:10.4049/jimmunol.0902749
26. S. A. FastQC: a quality control tool for high throughput sequence data. 2010;
27. Institute. JG. BMap guide. *JGI* . 10/23/2015 2015;
28. Dobin A, Davis CA, Schlesinger F, et al. STAR: ultrafast universal RNA-seq aligner. *Bioinformatics* . Jan 1 2013;29(1):15-21. doi:10.1093/bioinformatics/bts635
29. Anders S, Pyl PT, Huber W. HTSeq—a Python framework to work with high-throughput sequencing data. *Bioinformatics* . Jan 15 2015;31(2):166-9. doi:10.1093/bioinformatics/btu638
30. Love MI, Huber W, Anders S. Moderated estimation of fold change and dispersion for RNA-seq data with DESeq2. *Genome Biology* . 2014/12/05 2014;15(12):550. doi:10.1186/s13059-014-0550-8
31. Ge SX, Son EW, Yao R. iDEP: an integrated web application for differential expression and pathway analysis of RNA-Seq data. *BMC Bioinformatics* . 2018/12/19 2018;19(1):534. doi:10.1186/s12859-018-2486-6
32. Hänzelmann S, Castelo R, Guinney J. GSEA: gene set variation analysis for microarray and RNA-seq data. *BMC Bioinformatics* . Jan 16 2013;14:7. doi:10.1186/1471-2105-14-7
33. Daamen AR, Bachali P, Bonham CA, et al. COVID-19 patients exhibit unique transcriptional signatures indicative of disease severity. *Front Immunol* . 2022;13:989556. doi:10.3389/fimmu.2022.989556
34. Wilson JJ, Wei J, Daamen AR, et al. Glucose oxidation-dependent survival of activated B cells provides a putative novel therapeutic target for lupus treatment. *iScience* . Sep 15 2023;26(9):107487. doi:10.1016/j.isci.2023.107487
35. De Albuquerque N, Baig E, Ma X, et al. Murine hepatitis virus strain 1 produces a clinically relevant model of severe acute respiratory syndrome in A/J mice. *J Virol* . 2006/11// 2006;80(21):10382-10394. doi:10.1128/jvi.00747-06
36. DeAlbuquerque N, Baig E, Xuezhong M, et al. Murine Hepatitis Virus Strain 1 as a Model for Severe Acute Respiratory Distress Syndrome (Sars). Springer US; 2006:373-378.
37. Rai P, Chuong C, LeRoith T, et al. Adenovirus transduction to express human ACE2 causes obesity-specific morbidity in mice, impeding studies on the effect of host nutritional status on SARS-CoV-2 pathogenesis. *Virology* . Nov 2021;563:98-106. doi:10.1016/j.virol.2021.08.014
38. De Albuquerque N, Baig E, Ma X, et al. Murine hepatitis virus strain 1 produces a clinically relevant model of severe acute respiratory syndrome in A/J mice. *J Virol* . Nov 2006;80(21):10382-94. doi:10.1128/jvi.00747-06
39. VerHague M, Albright J, Barron K, Kim M, Bennett BJ. Obesogenic and diabetic effects of CD44 in mice are sexually dimorphic and dependent on genetic background. *Biology of Sex Differences* . 2022/04/11 2022;13(1):14. doi:10.1186/s13293-022-00426-2

40. Poggi M, Bastelica D, Gual P, et al. C3H/HeJ mice carrying a toll-like receptor 4 mutation are protected against the development of insulin resistance in white adipose tissue in response to a high-fat diet. *Diabetologia* . 2007/06/01 2007;50(6):1267-1276. doi:10.1007/s00125-007-0654-8
41. Almind K, Kahn CR. Genetic Determinants of Energy Expenditure and Insulin Resistance in Diet-Induced Obesity in Mice. *Diabetes* . 2004;53(12):3274-3285. doi:10.2337/diabetes.53.12.3274
42. Rendina-Ruedy E, Hembree KD, Sasaki A, et al. A Comparative Study of the Metabolic and Skeletal Response of C57BL/6J and C57BL/6N Mice in a Diet-Induced Model of Type 2 Diabetes. *J Nutr Metab* . 2015;2015:758080. doi:10.1155/2015/758080
43. Arulanandam B, Beladi H, Chakrabarti A. Obesity and COVID-19 mortality are correlated. *Scientific Reports* . 2023/04/11 2023;13(1):5895. doi:10.1038/s41598-023-33093-3
44. Bello-Chavolla OY, Bahena-López JP, Antonio-Villa NE, et al. Predicting Mortality Due to SARS-CoV-2: A Mechanistic Score Relating Obesity and Diabetes to COVID-19 Outcomes in Mexico. *J Clin Endocrinol Metab* . Aug 1 2020;105(8)doi:10.1210/clinem/dgaa346
45. Petersen A, Bressan K, Albrecht J, et al. The role of visceral adiposity in the severity of COVID-19: Highlights from a unicenter cross-sectional pilot study in Germany. *Metabolism* . Sep 2020;110:154317. doi:10.1016/j.metabol.2020.154317
46. Klang E, Kassim G, Soffer S, Freeman R, Levin MA, Reich DL. Severe Obesity as an Independent Risk Factor for COVID-19 Mortality in Hospitalized Patients Younger than 50. *Obesity (Silver Spring)* . Sep 2020;28(9):1595-1599. doi:10.1002/oby.22913
47. Bösmüller H, Matter M, Fend F, Tzankov A. The pulmonary pathology of COVID-19. *Virchows Arch* . Jan 2021;478(1):137-150. doi:10.1007/s00428-021-03053-1
48. Fox SE, Akmatbekov A, Harbert JL, Li G, Quincy Brown J, Vander Heide RS. Pulmonary and cardiac pathology in African American patients with COVID-19: an autopsy series from New Orleans. *Lancet Respir Med* . Jul 2020;8(7):681-686. doi:10.1016/s2213-2600(20)30243-5
49. Schaller T, Hirschi K, Burkhardt K, et al. Postmortem Examination of Patients With COVID-19. *Jama* . Jun 23 2020;323(24):2518-2520. doi:10.1001/jama.2020.8907
50. Barton LM, Duval EJ, Stroberg E, Ghosh S, Mukhopadhyay S. COVID-19 Autopsies, Oklahoma, USA. *Am J Clin Pathol* . May 5 2020;153(6):725-733. doi:10.1093/ajcp/aqaa062
51. Lax SF, Skok K, Zechner P, et al. Pulmonary Arterial Thrombosis in COVID-19 With Fatal Outcome : Results From a Prospective, Single-Center, Clinicopathologic Case Series. *Ann Intern Med* . Sep 1 2020;173(5):350-361. doi:10.7326/m20-2566
52. Carvallo FR, Stevenson VB. Interstitial pneumonia and diffuse alveolar damage in domestic animals. *Vet Pathol* . Jul 2022;59(4):586-601. doi:10.1177/03009858221082228
53. Sinha P, Bos LD. Pathophysiology of the Acute Respiratory Distress Syndrome: Insights from Clinical Studies. *Crit Care Clin* . Oct 2021;37(4):795-815. doi:10.1016/j.ccc.2021.05.005
54. van den Brand JM, Smits SL, Haagmans BL. Pathogenesis of Middle East respiratory syndrome coronavirus. *The Journal of Pathology* . 2015;235(2):175-184. doi:https://doi.org/10.1002/path.4458
55. Roberts CM, Levi M, McKee M, Schilling R, Lim WS, Grocott MPW. COVID-19: a complex multisystem disorder. *Br J Anaesth* . Sep 2020;125(3):238-242. doi:10.1016/j.bja.2020.06.013
56. Wang Y, Schughart K, Peláia TM, et al. Blood transcriptome responses in patients correlate with severity of COVID-19 disease. Original Research. *Frontiers in Immunology* . 2023-January-20 2023;13doi:10.3389/fimmu.2022.1043219

57. Mukhopadhyay S, Hoidal JR, Mukherjee TK. Role of TNF α in pulmonary pathophysiology. *Respir Res* . Oct 11 2006;7(1):125. doi:10.1186/1465-9921-7-125
58. Malaviya R, Laskin JD, Laskin DL. Anti-TNF α therapy in inflammatory lung diseases. *Pharmacol Ther* . Dec 2017;180:90-98. doi:10.1016/j.pharmthera.2017.06.008
59. Hanna A, Frangogiannis NG. Inflammatory Cytokines and Chemokines as Therapeutic Targets in Heart Failure. *Cardiovasc Drugs Ther* . Dec 2020;34(6):849-863. doi:10.1007/s10557-020-07071-0
60. Nawroth PP, Stern DM. Modulation of endothelial cell hemostatic properties by tumor necrosis factor. *J Exp Med* . Mar 1 1986;163(3):740-5. doi:10.1084/jem.163.3.740
61. Conkling PR, Greenberg CS, Weinberg JB. Tumor necrosis factor induces tissue factor-like activity in human leukemia cell line U937 and peripheral blood monocytes. *Blood* . Jul 1988;72(1):128-33.
62. Page EM, Ariens RAS. Mechanisms of thrombosis and cardiovascular complications in COVID-19. *Thromb Res* . Apr 2021;200:1-8. doi:10.1016/j.thromres.2021.01.005
63. Bautista-Vargas M, Bonilla-Abadía F, Cañas CA. Potential role for tissue factor in the pathogenesis of hypercoagulability associated with in COVID-19. *J Thromb Thrombolysis* . Oct 2020;50(3):479-483. doi:10.1007/s11239-020-02172-x
64. Kanneganti TD, Dixit VD. Immunological complications of obesity. *Nat Immunol* . Jul 19 2012;13(8):707-12. doi:10.1038/ni.2343
65. De Miguel C, Rudemiller NP, Abais JM, Mattson DL. Inflammation and hypertension: new understandings and potential therapeutic targets. *Curr Hypertens Rep* . Jan 2015;17(1):507. doi:10.1007/s11906-014-0507-z
66. Qiu D, Zhang D, Yu Z, Jiang Y, Zhu D. Bioinformatics approach reveals the critical role of the NOD-like receptor signaling pathway in COVID-19-associated multiple sclerosis syndrome. *J Neural Transm (Vienna)* . Aug 2022;129(8):1031-1038. doi:10.1007/s00702-022-02518-0
67. Zhao N, Di B, Xu LL. The NLRP3 inflammasome and COVID-19: Activation, pathogenesis and therapeutic strategies. *Cytokine Growth Factor Rev* . Oct 2021;61:2-15. doi:10.1016/j.cytogfr.2021.06.002
68. Uzun G, Pelzl L, Singh A, Bakchoul T. Immune-Mediated Platelet Activation in COVID-19 and Vaccine-Induced Immune Thrombotic Thrombocytopenia. Mini Review. *Frontiers in Immunology* . 2022-February-22 2022;13doi:10.3389/fimmu.2022.837629
69. Manne BK, Denorme F, Middleton EA, et al. Platelet gene expression and function in patients with COVID-19. *Blood* . Sep 10 2020;136(11):1317-1329. doi:10.1182/blood.2020007214
70. Pastorek M, Dúbrava M, Celec P. On the Origin of Neutrophil Extracellular Traps in COVID-19. *Front Immunol* . 2022;13:821007. doi:10.3389/fimmu.2022.821007
71. Al-Kuraishy HM, Al-Gareeb AI, Al-Hussaniy HA, Al-Harcan NAH, Alexiou A, Batiha GE. Neutrophil Extracellular Traps (NETs) and Covid-19: A new frontiers for therapeutic modality. *Int Immunopharmacol* . Mar 2022;104:108516. doi:10.1016/j.intimp.2021.108516
72. Ge J, Song T, Li M, et al. The medicinal value of tea drinking in the management of COVID-19. *Heliyon* . Jan 2023;9(1):e12968. doi:10.1016/j.heliyon.2023.e12968
73. Murphy KM, Ouyang W, Farrar JD, et al. Signaling and Transcription in T Helper Development. *Annual Review of Immunology* . 2000;18(1):451-494. doi:10.1146/annurev.immunol.18.1.451
74. Jason N, Xiaoyu L, Julie F, et al. SARS-CoV-2-specific T cells exhibit phenotypic features reflecting robust helper function, lack of terminal differentiation, and high proliferative potential. *bioRxiv* . 2020:2020.06.08.138826. doi:10.1101/2020.06.08.138826

75. Roncati L, Nasillo V, Lusenti B, Riva G. Signals of Th2 immune response from COVID-19 patients requiring intensive care. *Annals of Hematology* . 2020/06/01 2020;99(6):1419-1420. doi:10.1007/s00277-020-04066-7
76. Martonik D, Parfieniuk-Kowerda A, Rogalska M, Flisiak R. The Role of Th17 Response in COVID-19. *Cells* . Jun 19 2021;10(6)doi:10.3390/cells10061550
77. Zhao X, Liang Q, Li H, Jing Z, Pei D. Single-cell RNA sequencing and multiple bioinformatics methods to identify the immunity and ferroptosis-related biomarkers of SARS-CoV-2 infections to ischemic stroke. *Aging (Albany NY)* . Aug 21 2023;15(16):8237-8257. doi:10.18632/aging.204966
78. Wauters E, Van Mol P, Garg AD, et al. Discriminating mild from critical COVID-19 by innate and adaptive immune single-cell profiling of bronchoalveolar lavages. *Cell Research* . 2021/03/01 2021;31(3):272-290. doi:10.1038/s41422-020-00455-9
79. Gisby JS, Buang NB, Papadaki A, et al. Multi-omics identify falling LRRC15 as a COVID-19 severity marker and persistent pro-thrombotic signals in convalescence. *Nature Communications* . 2022/12/15 2022;13(1):7775. doi:10.1038/s41467-022-35454-4
80. Moolamalla STR, Balasubramanian R, Chauhan R, Priyakumar UD, Vinod PK. Host metabolic reprogramming in response to SARS-CoV-2 infection: A systems biology approach. *Microb Pathog* . Sep 2021;158:105114. doi:10.1016/j.micpath.2021.105114
81. Livanos AE, Jha D, Cossarini F, et al. Intestinal Host Response to SARS-CoV-2 Infection and COVID-19 Outcomes in Patients With Gastrointestinal Symptoms. *Gastroenterology* . Jun 2021;160(7):2435-2450.e34. doi:10.1053/j.gastro.2021.02.056
82. Daamen AR, Bachali P, Grammer AC, Lipsky PE. Classification of COVID-19 Patients into Clinically Relevant Subsets by a Novel Machine Learning Pipeline Using Transcriptomic Features. *Int J Mol Sci* . Mar 3 2023;24(5)doi:10.3390/ijms24054905
83. Aschenbrenner AC, Mouktaroudi M, Krämer B, et al. Disease severity-specific neutrophil signatures in blood transcriptomes stratify COVID-19 patients. *Genome Med* . Jan 13 2021;13(1):7. doi:10.1186/s13073-020-00823-5